Wind Simulations for the Gulf of Suez with KAMM

Frank, Helmut Paul

Publication date:
2003

Document Version
Publisher's PDF, also known as Version of record

RISØ

Risø-I-1970(EN)

Wind Simulations for the Gulf of Suez with KAMM

Helmut P. Frank

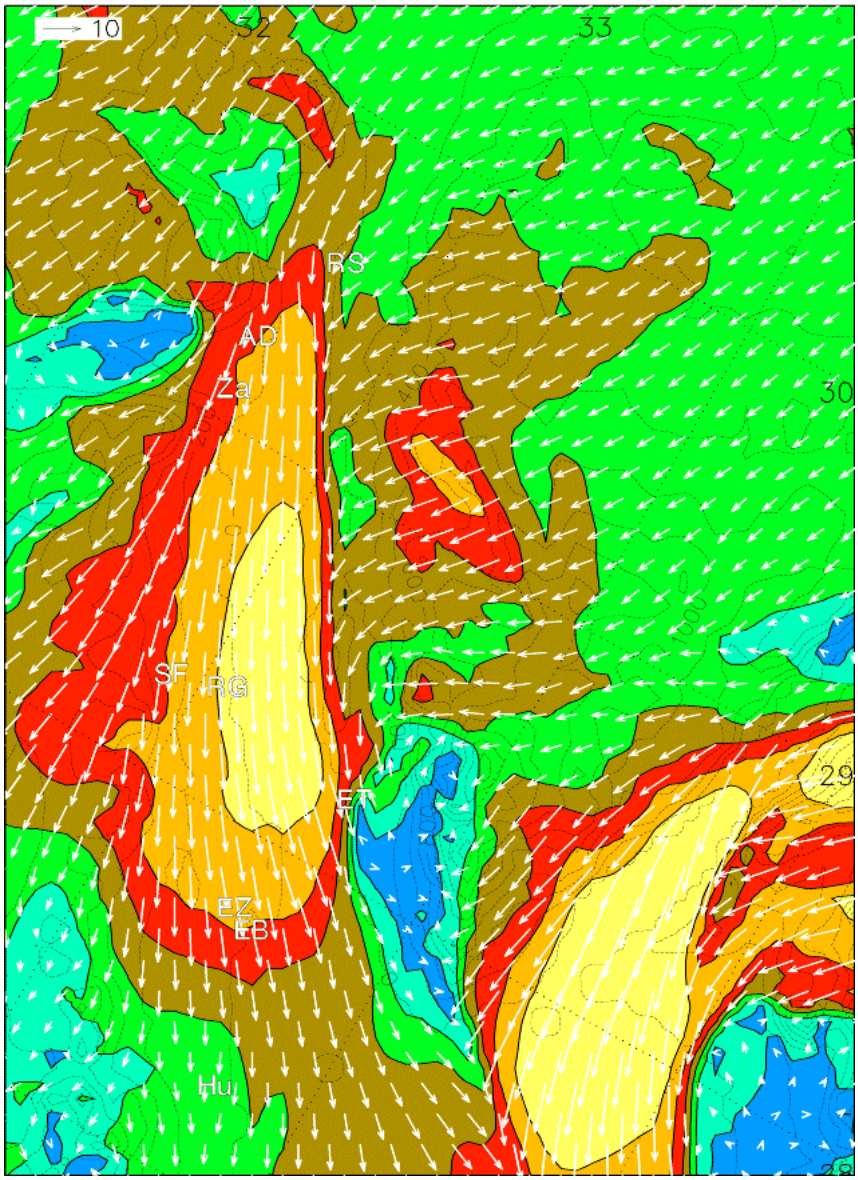

Risø National Laboratory, Roskilde, Denmark
April 2003

Risø-I-1970(EN)

Wind Simulations for the Gulf of Suez with KAMM

Helmut P. Frank

Risø National Laboratory, Roskilde
April 2003

Abstract In order to get a better overview of the spatial distribution of the wind resource in the Gulf of Suez, numerical simulations to determine the wind climate have been carried out with the Karlsruhe Atmospheric Mesoscale Model KAMM. The method and the results are described here.

The simulations of the wind climate of the Gulf of Suez with KAMM capture the main features of the observed wind climate. The mean wind speed and energy flux density are somewhat underpredicted.

The present report is a result of the Egyptian-Danish project *Wind Atlas for Egypt*. This project and the publication of the report are funded by the Danish Ministry of Foreign Affairs through Danida.

Print: Pitney Bowes Management Services Danmark A/S, 2003

Wind Simulations for the Gulf of Suez with KAMM

Helmut P. Frank

Risø National Laboratory
Wind Energy and Atmospheric Physics Department
Roskilde, Denmark

26 April 2000

1 Introduction

In order to get a better overview of the special distribution of the wind resource in the Gulf of Suez, numerical simulations to determine the wind climate have been carried out with the Karlsruhe Atmospheric Mesoscale Model KAMM (Adrian and Fiedler, 1991; Adrian, 1994). The method and the results are described here.

2 Model domain

The model domain has 60×81 grid points with a grid size of 5 km. An orographic map of the area is shown in Figure 1. Three grid points at a boundary in direction orthogonal to the boundary must have the same height to allow free propagation of gravity waves out of the model domain. The map is rotated 30° relative to true north to align the axis of the Gulf with the a side of the model. Then the boundary condition for the orography does not introduce an unrealistic kink near the boundaries. A grid of latitude and longitude is shown by thin, dotted lines.

The model uses 28 levels in the vertical from the surface to a constant height of 6000 m a.s.l.. The resolution is greater near the surface than at the top of the model. The height of some levels above a grid point at sea level are listed below:

level	z [m]
1	6000
2	5572
3	5150
22	337.0
23	241.3
24	161.4
25	97.3
26	49.1
27	16.6
28	0.0

3 Initial Data

The method of statistical-dynamical down scaling (Frey-Buness et al., 1995) is used to determine the wind climate on the meso-scale from large-scale data (see e.g. Frank and Landberg, 1997, 1998).

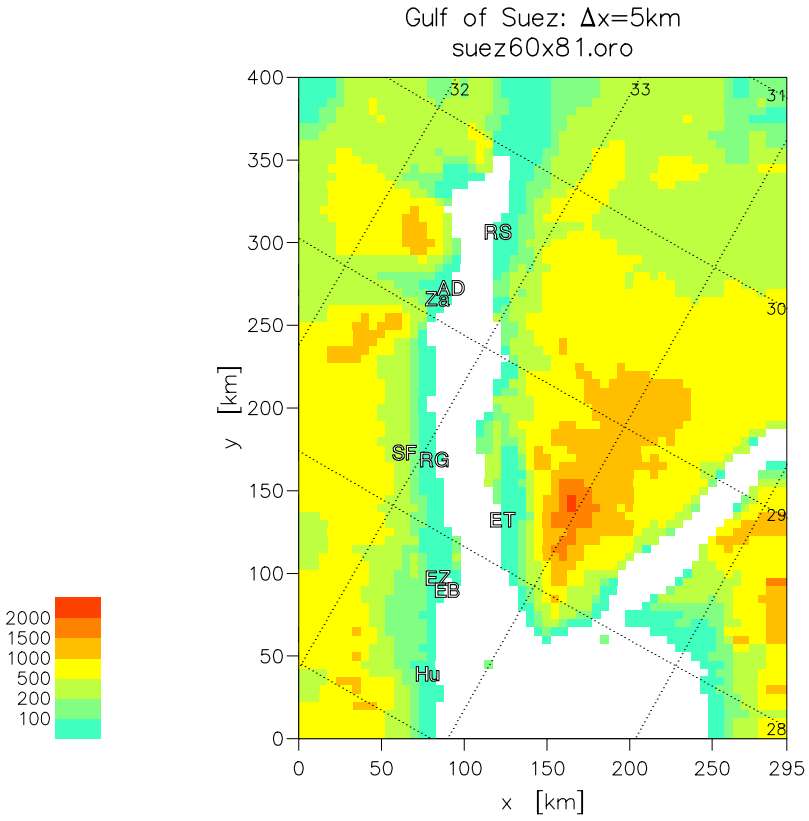

Figure 1: Orography for the simulations.

128 simulations with different base state, i.e. initial data, are made. The base state is given by the geostrophic wind and temperature at 4 heights: 0 m, 1500 m, 3000 m, 5500 m. The values are determined from the NCEP/NCAR global reanalysis (Kalnay et al., 1996) for the years 1965–1998 at the pressure levels 1000 hPa, 850 hPa, 700 hPa, and 500 hPa. The 128 classes are determined from 16 sectors of the geostrophic wind at 0 m and positive or negative shear between the geostrophic wind at 0 m and 1500 m. At greater heights the geostrophic wind always increases and becomes more westerly. The 128 classes are listed in Table 1.

Table 1: Simulation IDs, speed and direction of the geostrophic wind at sea level, shear between 0 m and 1500 m, frequencies of this wind class, and simulation time for the 128 simulations.

ID	DD [°]	v_h [m s^{-1}]	Shear [m s^{-1}]	Freq. [%]	sim.time [min]
SU4Z000020	8	2.01	2.013	0.560	760
SU4Z000039	3	3.94	−1.889	0.169	670
SU4Z000035	6	3.52	2.172	0.560	690
SU4Z000055	3	5.47	−1.954	0.354	610
SU4Z000052	5	5.22	2.371	0.556	620
SU4Z000067	4	6.71	−2.097	0.374	560
SU4Z000065	4	6.50	2.472	0.399	570
SU4Z000081	4	8.07	−2.307	0.580	510
SU4Z000079	4	7.86	2.594	0.258	520
SU4Z000101	3	10.05	−2.472	0.680	450
SU4Z000100	2	9.98	2.922	0.165	460

ID	DD	v_h	Shear	Freq.	sim.time
SU4Z000130	3	13.00	-1.922	0.342	390
SU4Z023026	30	2.58	1.706	1.059	740
SU4Z023049	27	4.92	-1.989	0.825	630
SU4Z023045	27	4.52	2.352	1.236	650
SU4Z023065	25	6.54	-2.256	1.530	570
SU4Z023063	25	6.30	2.567	0.499	580
SU4Z023081	26	8.10	-2.449	1.812	510
SU4Z023078	25	7.76	2.622	0.205	530
SU4Z023095	27	9.53	-2.552	1.953	470
SU4Z023093	26	9.27	2.982	0.129	480
SU4Z023116	27	11.57	-2.748	1.973	410
SU4Z023113	24	11.28	3.351	0.032	420
SU4Z023149	27	14.89	-3.012	0.809	390
SU4Z045032	49	3.20	1.066	2.376	710
SU4Z045059	47	5.90	-2.265	3.652	590
SU4Z045055	47	5.47	2.552	0.958	610
SU4Z045077	47	7.68	-2.461	4.288	530
SU4Z045073	44	7.34	2.511	0.270	540
SU4Z045093	46	9.28	-2.619	4.530	480
SU4Z045088	45	8.84	2.737	0.032	490
SU4Z045109	46	10.88	-2.747	4.558	430
SU4Z045130	46	12.95	-2.929	4.590	390
SU4Z045163	46	16.34	-3.190	1.812	390
SU4Z068031	69	3.13	0.930	1.840	710
SU4Z068055	68	5.45	-2.276	3.020	610
SU4Z068050	69	5.00	2.535	0.636	630
SU4Z068072	67	7.15	-2.427	3.551	550
SU4Z068067	68	6.71	2.494	0.129	560
SU4Z068087	67	8.64	-2.533	3.684	500
SU4Z068102	66	10.18	-2.704	3.624	450
SU4Z068122	66	12.22	-2.830	3.616	390
SU4Z068156	65	15.58	-3.126	1.466	390
SU4Z090025	91	2.52	1.424	0.986	740
SU4Z090045	90	4.54	-2.157	1.236	650
SU4Z090042	89	4.24	2.684	0.568	660
SU4Z090062	89	6.18	-2.365	1.925	580
SU4Z090058	91	5.78	2.602	0.093	600
SU4Z090075	89	7.46	-2.388	1.687	540
SU4Z090090	88	8.96	-2.547	1.888	490
SU4Z090110	88	10.98	-2.718	1.780	430
SU4Z090141	87	14.10	-2.954	0.729	390
SU4Z113021	110	2.09	1.541	0.487	760
SU4Z113040	110	3.99	-2.082	0.596	670
SU4Z113037	109	3.74	2.587	0.407	680
SU4Z113055	109	5.49	-2.274	0.825	610
SU4Z113054	110	5.40	2.931	0.077	610

ID	DD	v_h	Shear	Freq.	sim.time
SU4Z113068	112	6.82	-2.376	0.930	560
SU4Z113066	107	6.64	2.708	0.040	570
SU4Z113081	112	8.13	-2.433	0.934	510
SU4Z113102	110	10.15	-2.610	0.958	450
SU4Z113135	109	13.46	-2.855	0.378	390
SU4Z135017	130	1.72	1.597	0.342	780
SU4Z135038	134	3.76	-1.886	0.366	680
SU4Z135037	132	3.71	2.512	0.250	680
SU4Z135056	133	5.60	-2.231	0.572	600
SU4Z135053	134	5.27	2.889	0.040	620
SU4Z135073	133	7.28	-2.417	0.616	540
SU4Z135067	132	6.71	3.117	0.020	560
SU4Z135095	133	9.51	-2.569	0.612	470
SU4Z135125	133	12.54	-2.811	0.254	390
SU4Z158021	149	2.11	1.530	0.262	760
SU4Z158041	154	4.11	-1.970	0.326	670
SU4Z158039	153	3.87	2.367	0.201	680
SU4Z158062	153	6.20	-2.299	0.459	580
SU4Z158059	154	5.87	2.447	0.072	590
SU4Z158092	156	9.18	-2.539	0.503	480
SU4Z158083	160	8.30	2.920	0.024	510
SU4Z158136	156	13.56	-2.990	0.213	390
SU4Z180023	173	2.33	1.634	0.354	750
SU4Z180069	177	6.92	-2.246	0.451	550
SU4Z180057	178	5.74	2.393	0.262	600
SU4Z180118	177	11.83	-2.221	0.278	400
SU4Z203020	195	1.96	1.744	0.254	770
SU4Z203067	198	6.66	-2.055	0.177	560
SU4Z203055	199	5.46	2.148	0.318	610
SU4Z203120	200	11.99	-1.153	0.189	400
SU4Z225012	213	1.19	2.120	0.234	810
SU4Z225053	218	5.29	-1.706	0.032	620
SU4Z225044	222	4.39	2.032	0.391	650
SU4Z225115	223	11.52	0.830	0.177	410
SU4Z248014	241	1.39	2.100	0.246	790
SU4Z248056	244	5.63	-1.380	0.020	600
SU4Z248046	246	4.65	2.042	0.443	640
SU4Z248111	247	11.06	1.472	0.189	420
SU4Z270015	268	1.51	1.923	0.282	790
SU4Z270044	268	4.35	-1.118	0.020	660
SU4Z270042	271	4.16	2.121	0.431	660
SU4Z270082	271	8.14	1.655	0.471	510
SU4Z270136	272	13.57	1.542	0.197	390
SU4Z293014	297	1.34	2.103	0.254	800
SU4Z293037	298	3.71	-1.287	0.036	680
SU4Z293035	295	3.46	2.174	0.443	690

ID	DD	v_h	Shear	Freq.	sim.time
SU4Z293067	294	6.70	-1.342	0.048	560
SU4Z293062	296	6.22	2.087	0.439	580
SU4Z293106	292	10.63	-1.381	0.085	440
SU4Z293098	295	9.78	2.045	0.395	460
SU4Z293156	294	15.57	1.528	0.193	390
SU4Z315013	323	1.34	2.090	0.270	800
SU4Z315037	318	3.67	-1.318	0.032	690
SU4Z315030	321	3.03	2.141	0.435	710
SU4Z315049	321	4.93	-1.428	0.052	630
SU4Z315052	321	5.18	2.160	0.431	620
SU4Z315079	319	7.87	-1.698	0.101	520
SU4Z315077	318	7.71	2.386	0.391	530
SU4Z315110	317	11.01	-1.807	0.121	430
SU4Z315106	316	10.58	2.352	0.362	440
SU4Z315155	313	15.54	0.984	0.197	390
SU4Z338017	349	1.74	1.922	0.334	780
SU4Z338037	343	3.65	-1.648	0.052	690
SU4Z338034	344	3.35	2.082	0.507	700
SU4Z338054	339	5.44	-1.831	0.121	610
SU4Z338051	341	5.15	2.301	0.483	620
SU4Z338072	341	7.22	-2.143	0.234	540
SU4Z338069	342	6.92	2.407	0.362	560
SU4Z338098	341	9.83	-2.267	0.250	460
SU4Z338093	341	9.33	2.567	0.330	470
SU4Z338137	338	13.70	-0.641	0.242	390

The geostrophic wind at 0 m and the frequency of the corresponding class are shown in Figure 2. The geostrophic wind at 0 m , 1500 m, 3000 m is shown in Figure 3. This shows that easterlies and northeasterlies dominate at the surface. But, at 3000 m (and 5500 m) only westerly winds are present.

The horizontal variation of the large-scale geostrophic wind is shown in Figures 4 and 5. At sea level the geostrophic wind increases towards the south, and at 1500 m a.s.l. it decreases towards the south. Again, the geostrophic wind at 1500 m is much weaker than at sea level.

For weak forcing, i.e. weak geostrophic wind, the simulations take longer to reach a quasi-stationary state. Therefore, the simulation time depends on the speed of the geostrophic wind:

$$t = \max(870e^{-0.065U}, 390)\text{min}$$

with magnitude of the geostrophic wind U in m s^{-1}. This yields simulation times from 6.5 h to 13.5 h.

For all simulations the land surface temperature is specified to be 8 K warmer than the initial air temperature at the surface, and the sea surface temperature is 3 K warmer than the initial air temperature. In reality the temperature difference, which determines the stratification of the surface layer, depends on the time of the day and the season.

4 Results

4.1 Results of individual simulations

The wind fields at the end of the simulation time for some of the 128 classes are shown in the following figures. Shown is the wind speed at 25 m a.g.l. in colors and arrows of the horizontal

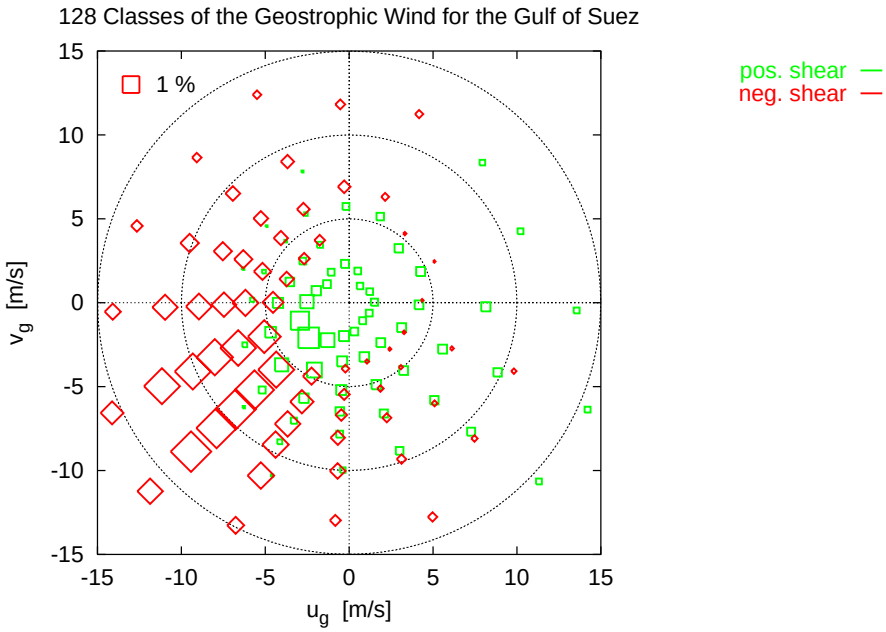

Figure 2: Geostrophic wind classes and frequencies of the classes

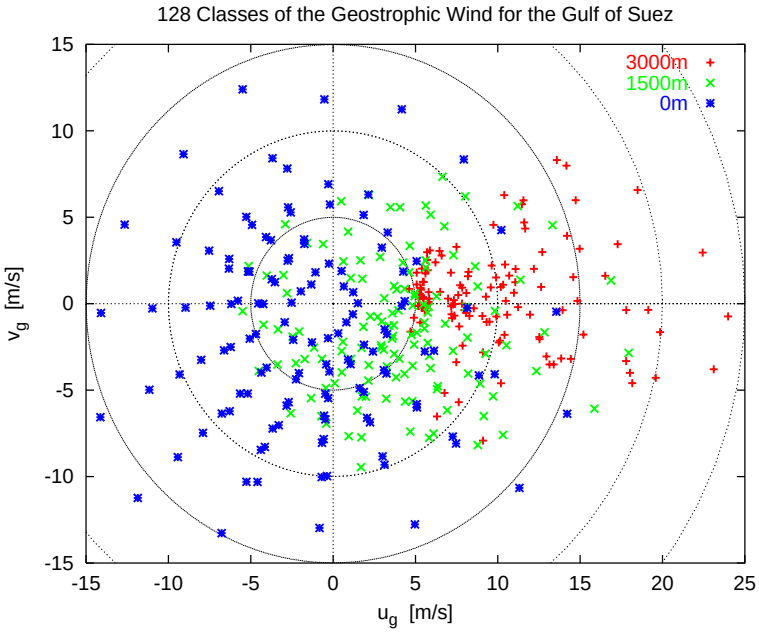

Figure 3: Components of the geostrophic wind at 0 m, 1500 m, and 3000 m for the 128 geostrophic wind classes.

wind vector. The ID of the simulation is written in the upper left corner. The indicated time is not correct. It is only an average simulation time for all simulations.

Two simulations next to each other are always from the same sector. For most pairs the left plot shows a class with negative shear, and the right plot one with positive shear between 0 m and 1500 m of the base state. The geostrophic wind at the surface is almost the same for these cases. The location of the area with the highest winds depends on the shear. For geostrophic wind from the northeasterly sector the highest winds occur further south in simulations with positive shear than in simulations with negative shear.

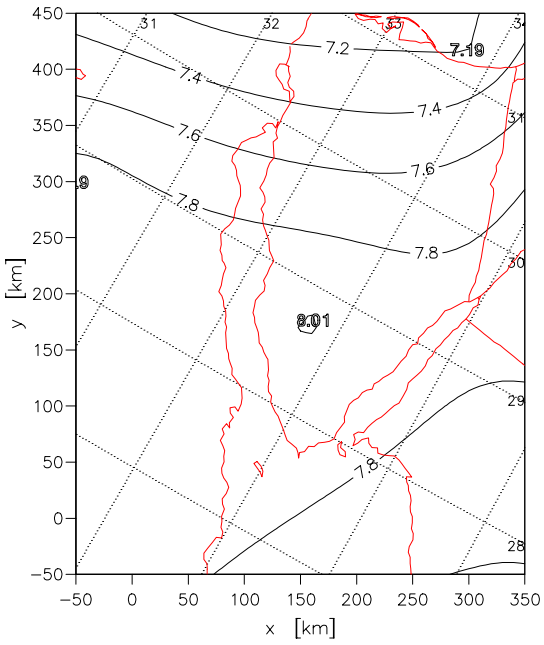

Figure 4: Magnitude of the geostrophic wind at 0 m a.s.l. in the Gulf of Suez area for the years 1965-98 of the NCEP/NCAR reanalysis. The geostrophic wind is calculated with the Coriolis parameter at latitude $28.75°$ N.

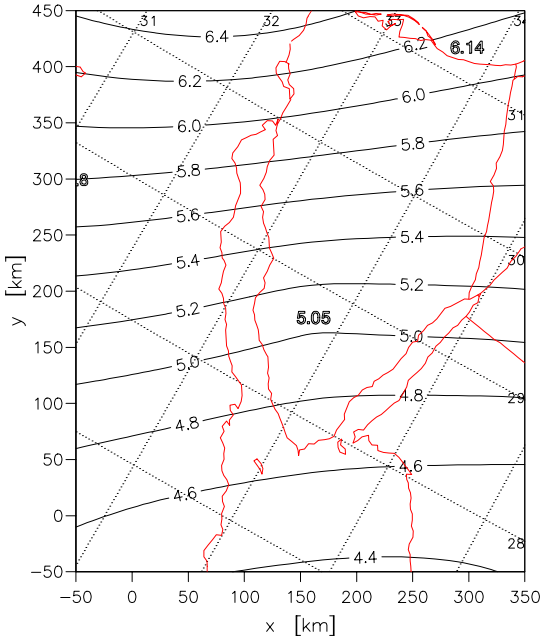

Figure 5: Magnitude of the geostrophic wind at 1500 m a.s.l. for the years 1965-98 of the NCEP/NCAR reanalysis.

Egypt/KAMM/Suez.Stat
SU4Z000067.out1.db
t= 7.0h
vh
z= 25m agl.

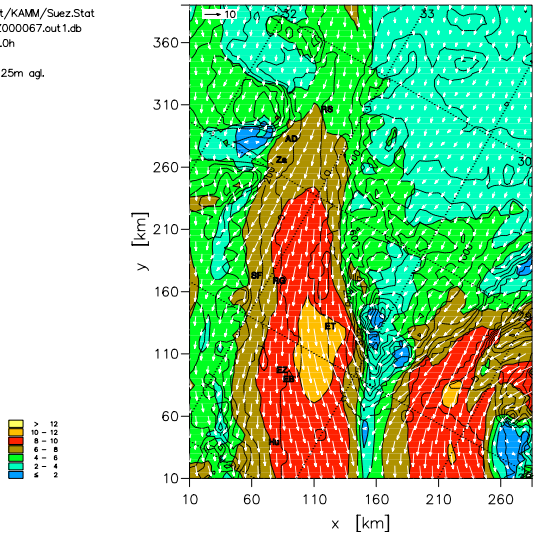

Egypt/KAMM/Suez.Stat
SU4Z000065.out1.db
t= 7.0h
vh
z= 25m agl.

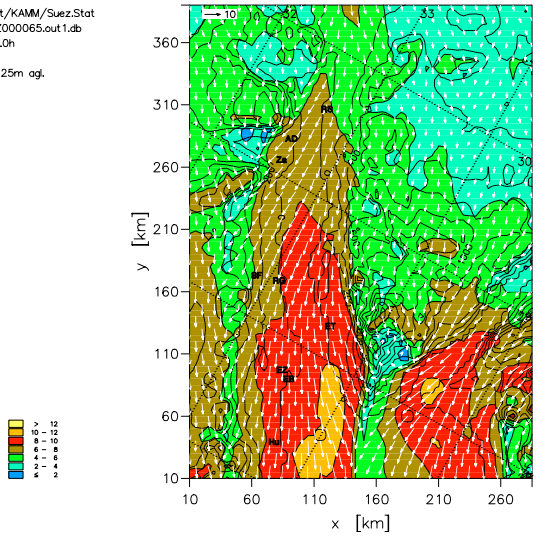

Egypt/KAMM/Suez.Stat
SU4Z023049.out1.db
t= 7.0h
vh
z= 25m agl.

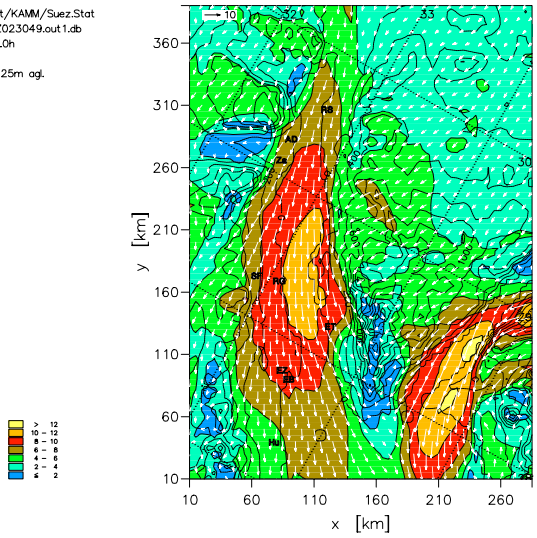

Egypt/KAMM/Suez.Stat
SU4Z023045.out1.db
t= 7.0h
vh
z= 25m agl.

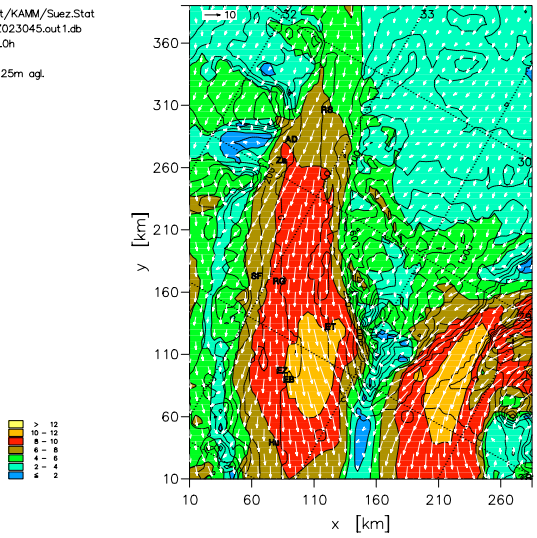

Egypt/KAMM/Suez.Stat
SU4Z045093.out1.db
t= 7.0h
vh
z= 25m agl.

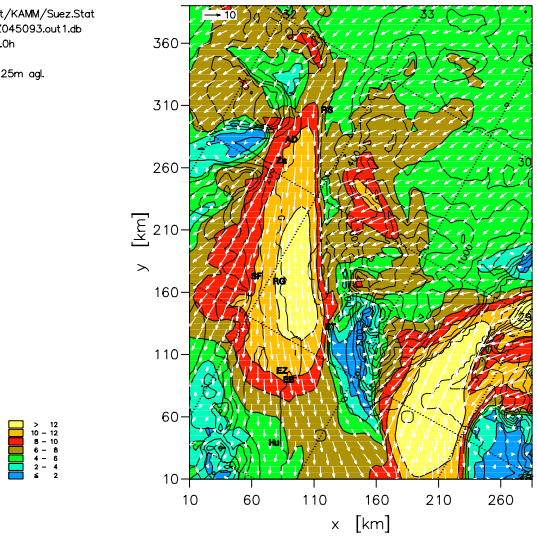

Egypt/KAMM/Suez.Stat
SU4Z045088.out1.db
t= 7.0h
vh
z= 25m agl.

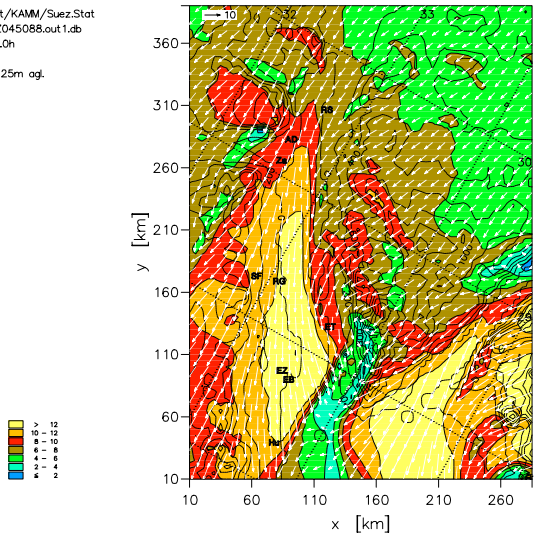

Egypt/KAMM/Suez.Stat
SU4Z068072.out1.db
t= 7.0h
vh
z= 25m agl.

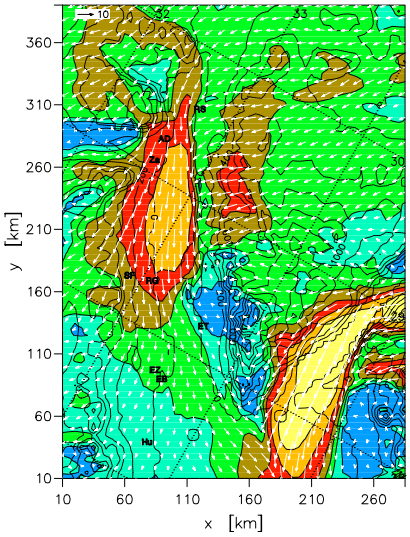

Egypt/KAMM/Suez.Stat
SU4Z068067.out1.db
t= 7.0h
vh
z= 25m agl.

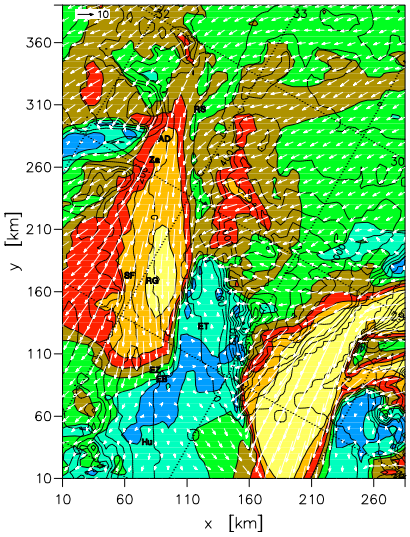

Egypt/KAMM/Suez.Stat
SU4Z090045.out1.db
t= 7.0h
vh
z= 25m agl.

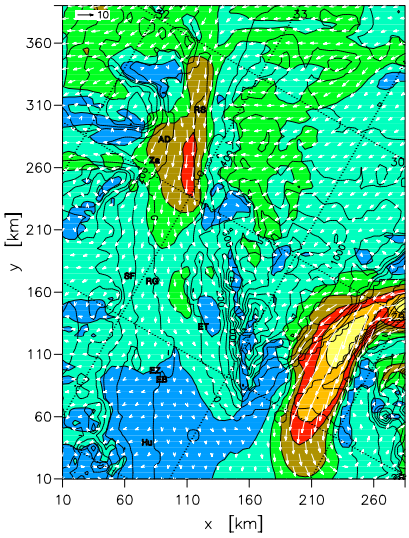

Egypt/KAMM/Suez.Stat
SU4Z090042.out1.db
t= 7.0h
vh
z= 25m agl.

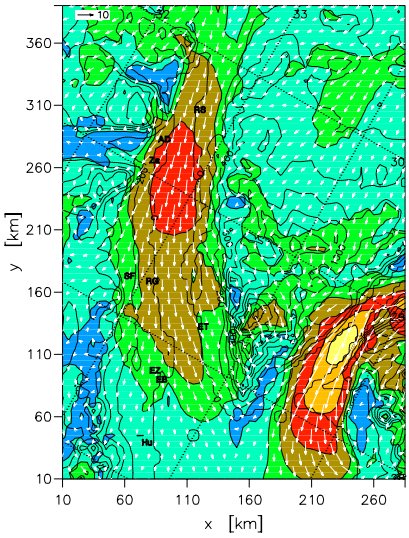

Egypt/KAMM/Suez.Stat
SU4Z113068.out1.db
t= 7.0h
vh
z= 25m agl.

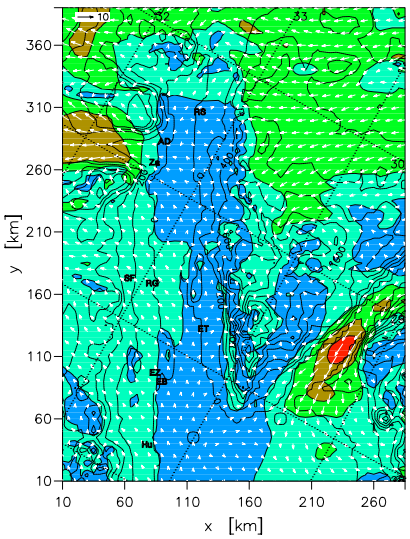

Egypt/KAMM/Suez.Stat
SU4Z113066.out1.db
t= 7.0h
vh
z= 25m agl.

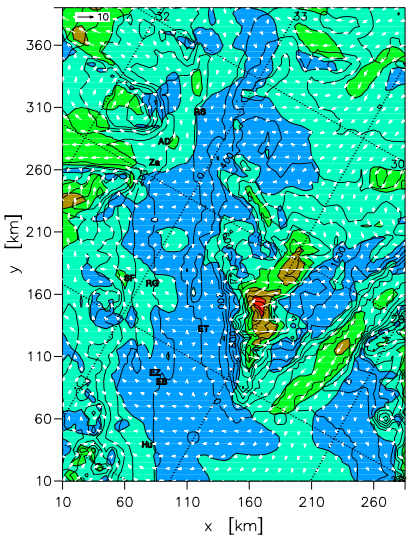

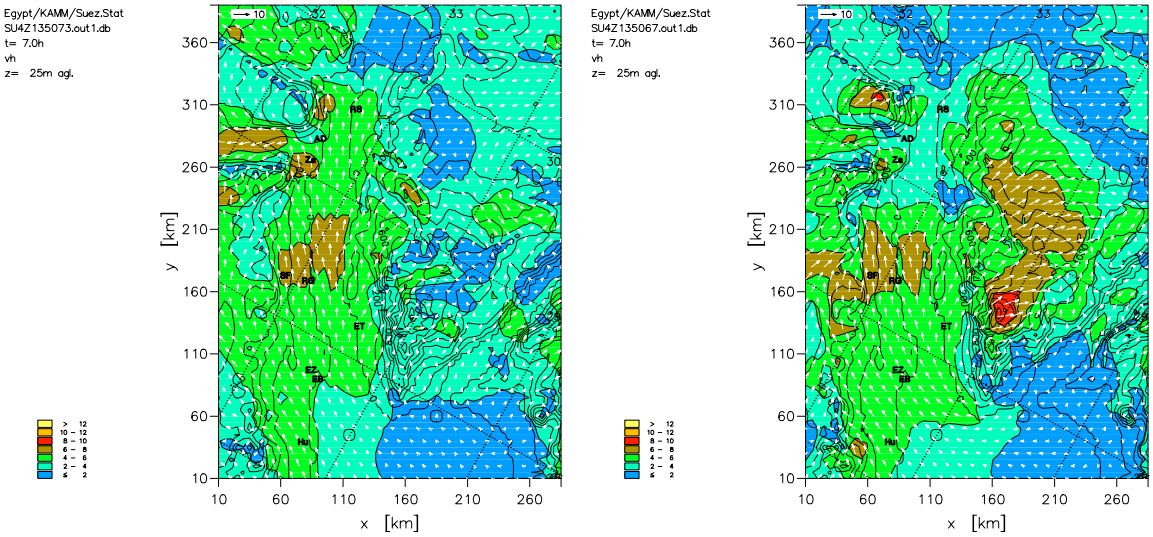
Egypt/KAMM/Suez.Stat
SU4Z135073.out1.db
t= 7.0h
vh
z= 25m agl.
Egypt/KAMM/Suez.Stat
SU4Z135067.out1.db
t= 7.0h
vh
z= 25m agl.
y [km]
x [km]

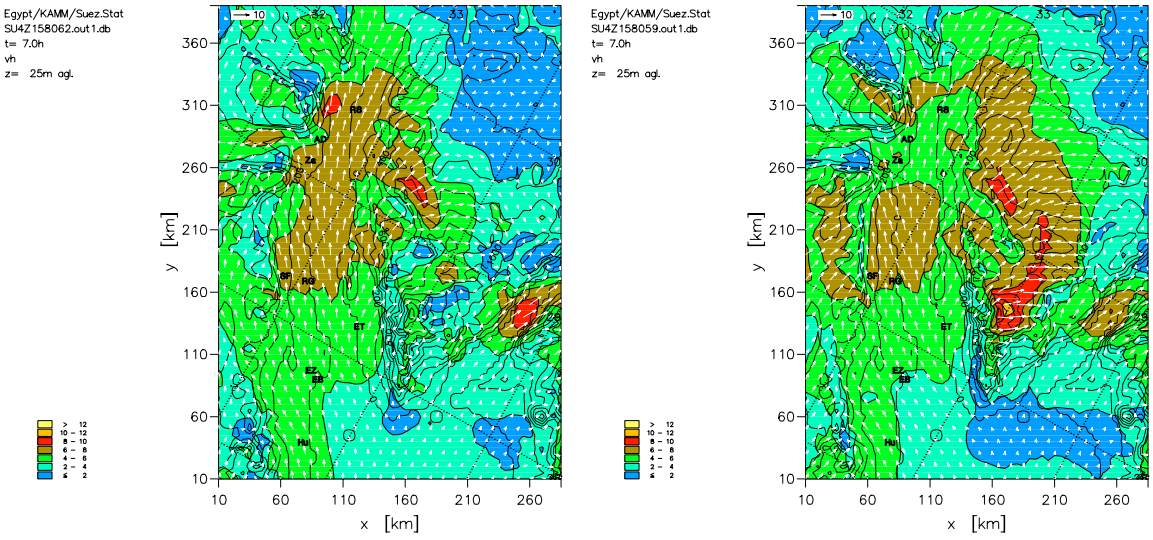
Egypt/KAMM/Suez.Stat
SU4Z158062.out1.db
t= 7.0h
vh
z= 25m agl.
Egypt/KAMM/Suez.Stat
SU4Z158059.out1.db
t= 7.0h
vh
z= 25m agl.
y [km]
x [km]

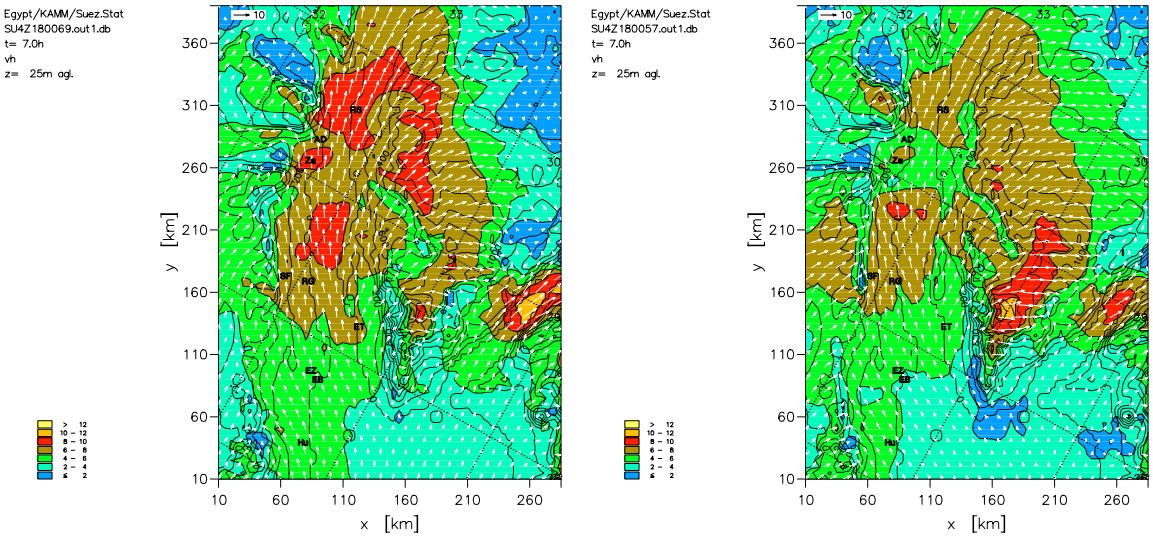
Egypt/KAMM/Suez.Stat
SU4Z180069.out1.db
t= 7.0h
vh
z= 25m agl.
Egypt/KAMM/Suez.Stat
SU4Z180057.out1.db
t= 7.0h
vh
z= 25m agl.
y [km]
x [km]

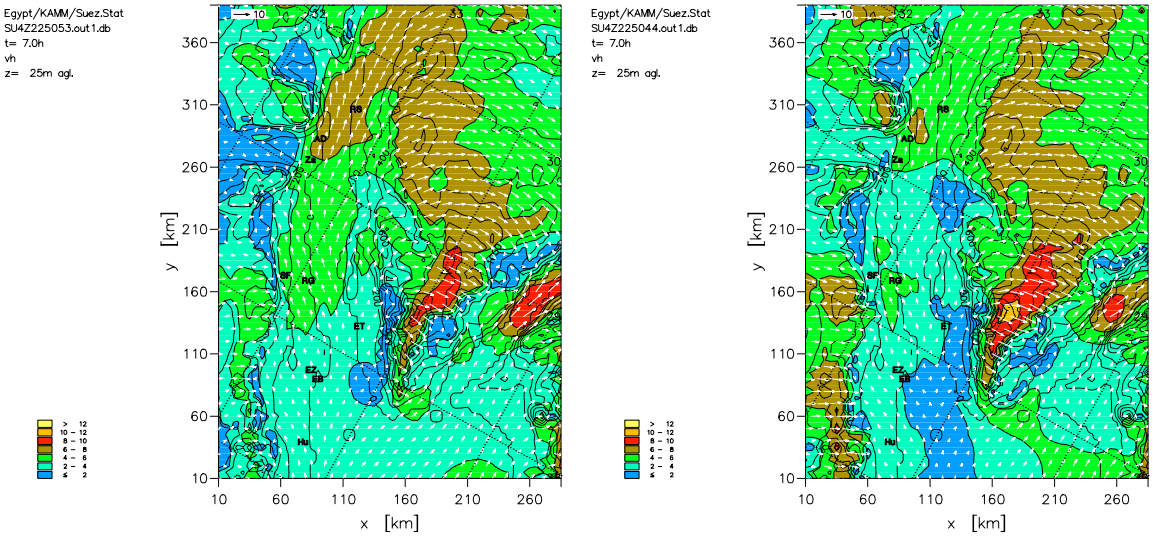
Egypt/KAMM/Suez.Stat
SU4Z225053.out1.db
t= 7.0h
vh
z= 25m agl.
Egypt/KAMM/Suez.Stat
SU4Z225044.out1.db
t= 7.0h
vh
z= 25m agl.
Egypt/KAMM/Suez.Stat
SU4Z270044.out1.db
t= 7.0h
vh
z= 25m agl.
Egypt/KAMM/Suez.Stat
SU4Z270042.out1.db
t= 7.0h
vh
z= 25m agl.
Egypt/KAMM/Suez.Stat
SU4Z293067.out1.db
t= 7.0h
vh
z= 25m agl.
Egypt/KAMM/Suez.Stat
SU4Z293062.out1.db
t= 7.0h
vh
z= 25m agl.
x [km]
y [km]

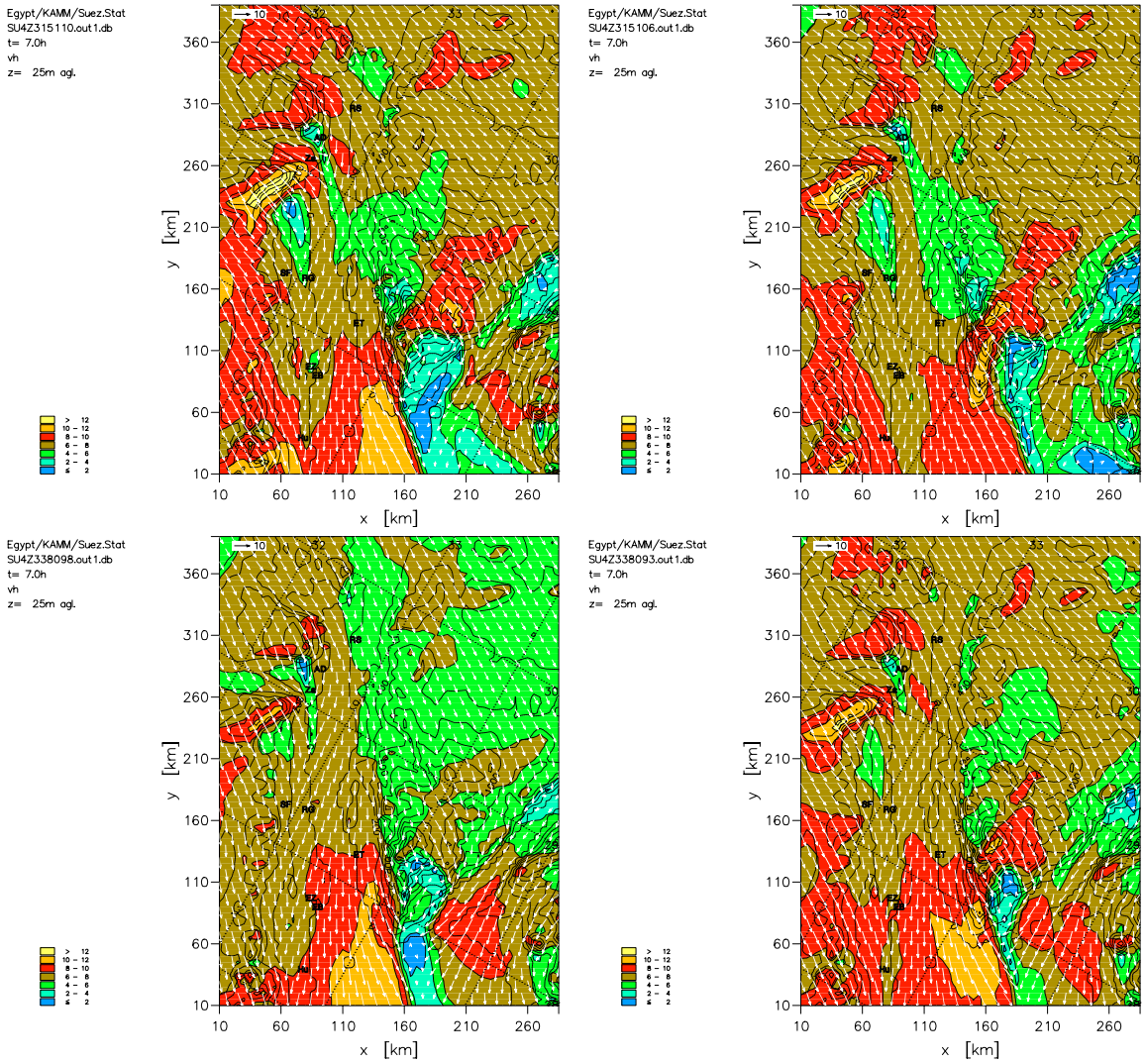

Time series of wind speed and direction at the first level above the surface at 12 grid points are shown in the following plots. The height above the surface is approximately 16 m. It is interesting that for some simulation the wind does not reach a steady state, even after many hours of simulation. This is especially the case for the grid points in the south near the Gulf of El-Zayt, Ras El-Behar and at Hurghada. Also, the simulations with negative shear seem to be further away from a steady state than those with positive shear.

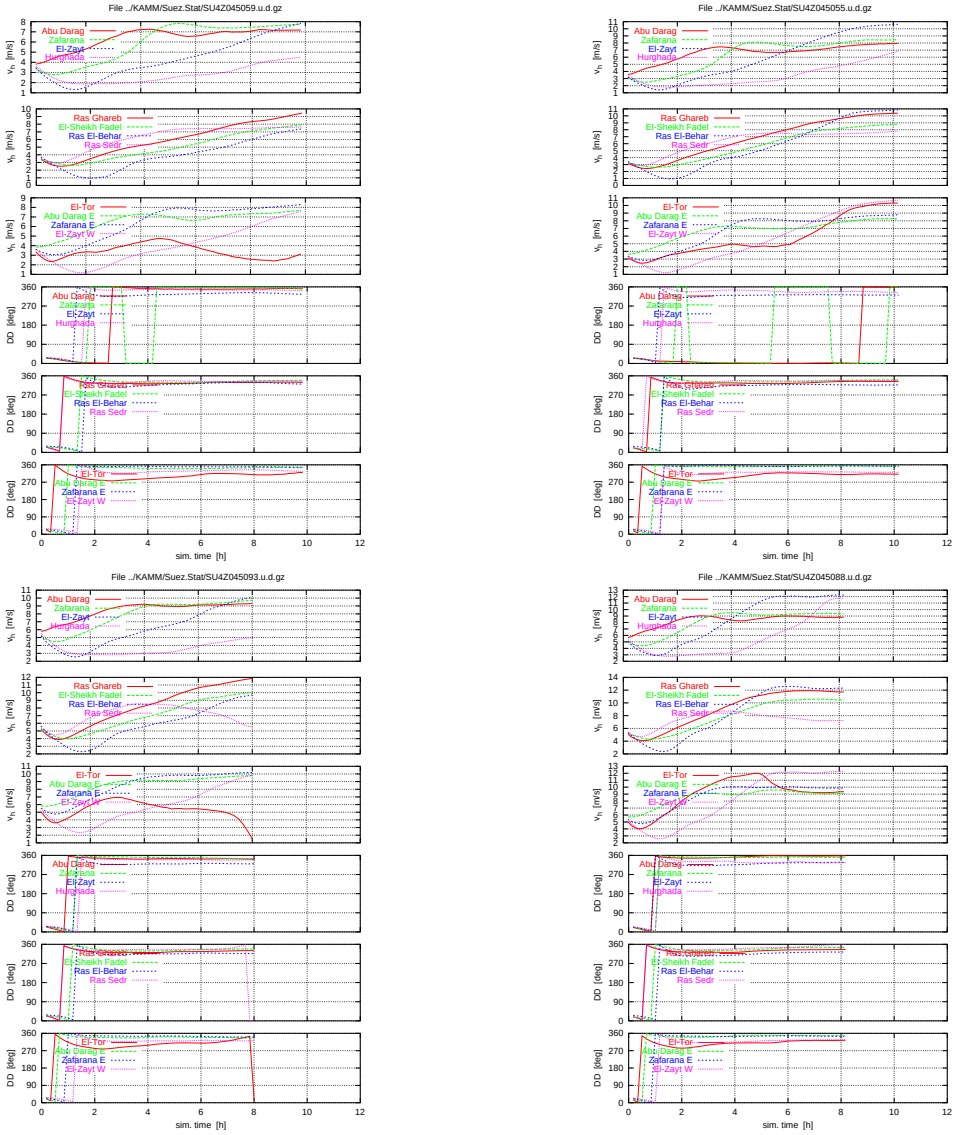

4.2 Mean wind and energy flux density

Figures 6 and 7 show the average wind speed and energy flux density at 25 m a.g.l. over the local roughness (typically 2 mm in the desert). The maximum occurs in the center of the Gulf towards the west side over water.

Figures 8 and 9 show wind speed and energy flux density at 25 m a.g.l. transformed to a uniform roughness of 0.2 mm. Now, the maximum lies slightly further west over land.

The simulations predict even higher wind for the Gulf of Aqaba than for the Gulf of Suez. However, these results are less reliable, because this valley is not fully included in the simulation domain. The northeastern part of the Gulf of Aqaba is cut off at the righ side of the domain.

4.3 Wind roses

The wind roses and Weibull distributions for a height of $z = 25$ m over roughness class 0 ($z_0 = 0.2$ mm) from the observations are shown below.

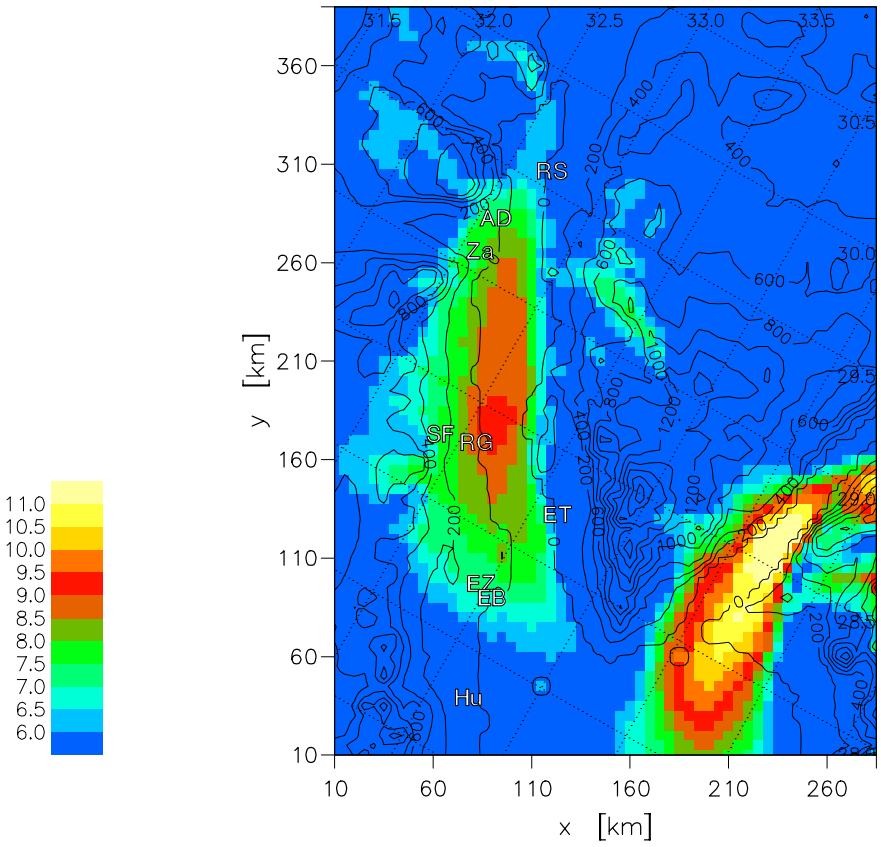

Figure 6: U [m s^{-1}] at 25 m over the local roughness z_0.

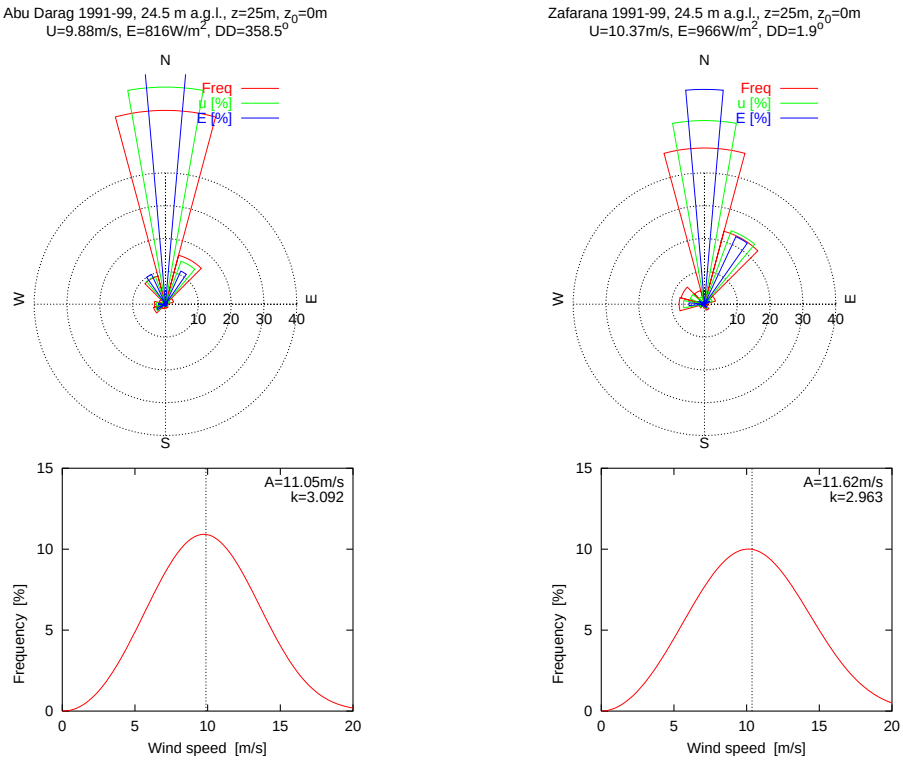

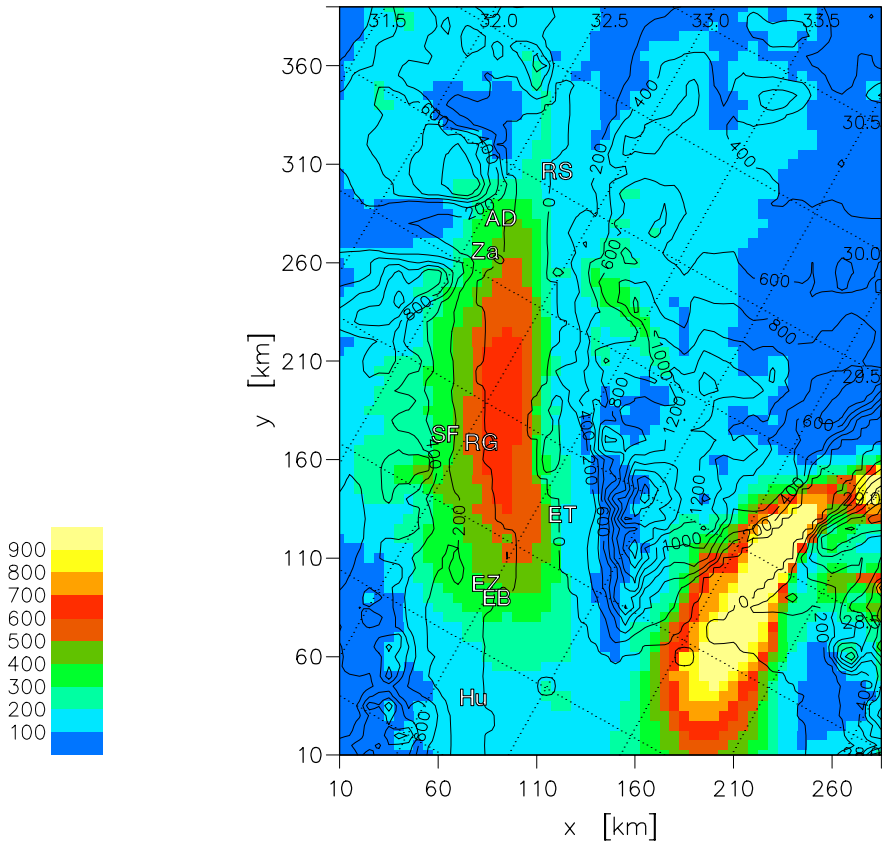

Figure 7: E [W m^{-2}] at 25 m over the local roughness z_0.

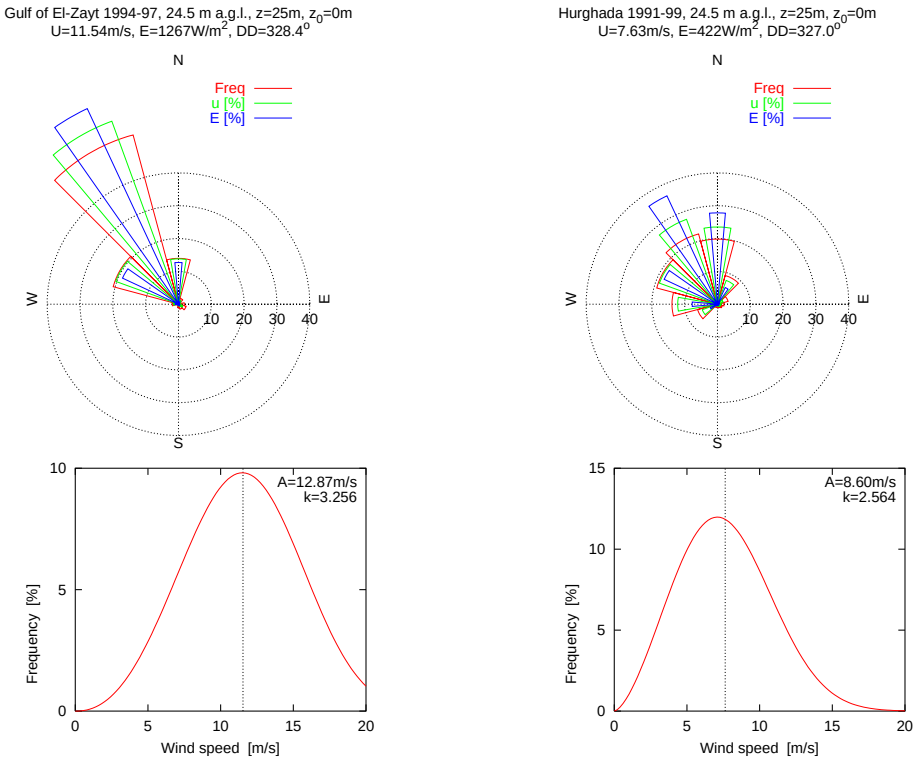

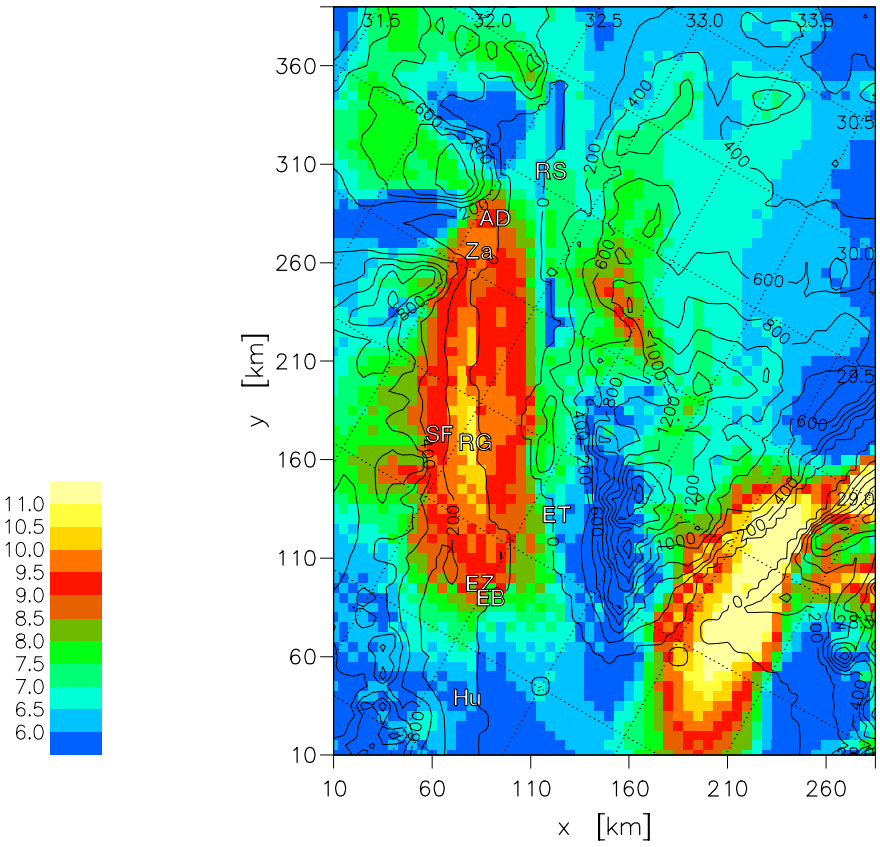

Figure 8: U [m s^{-1}] at 25 m over $z_0 = 0.2$ mm.

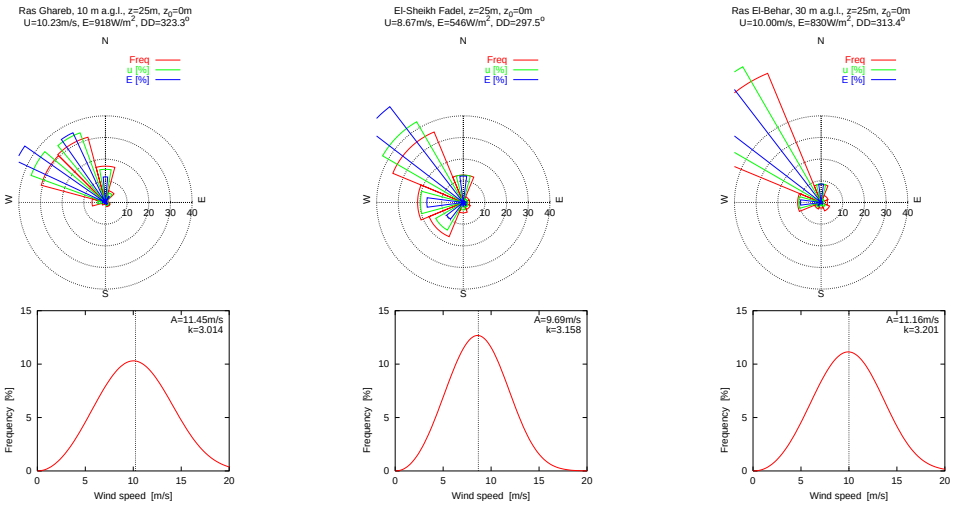

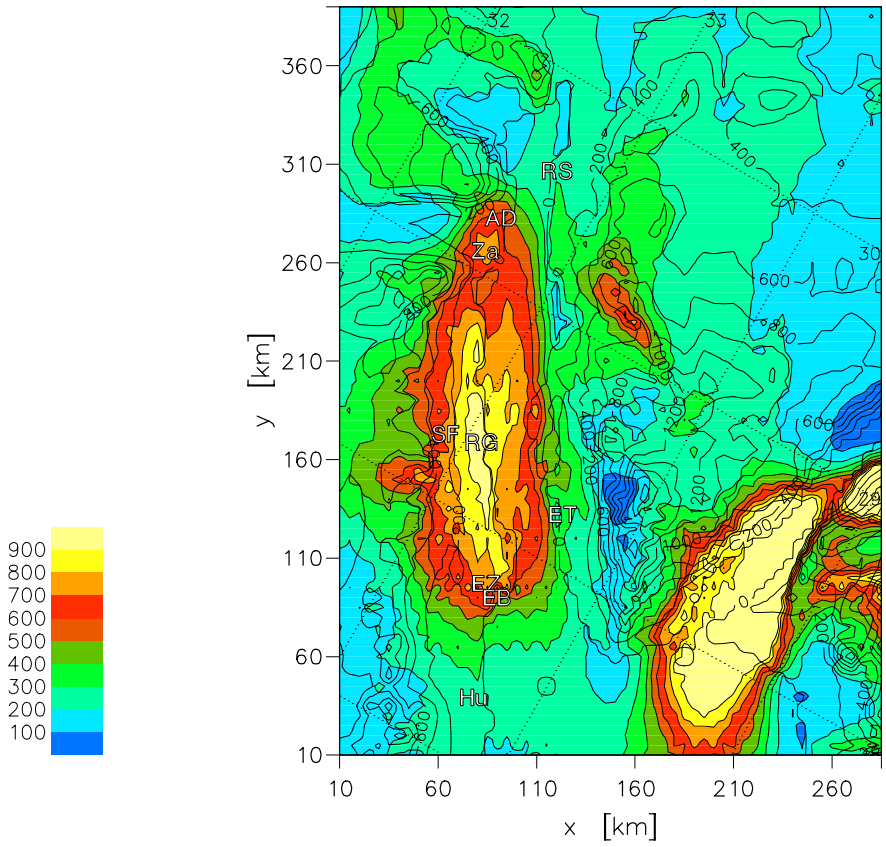

Figure 9: E [W m^{-2}] at 25 m over $z_0 = 0.2$ mm.

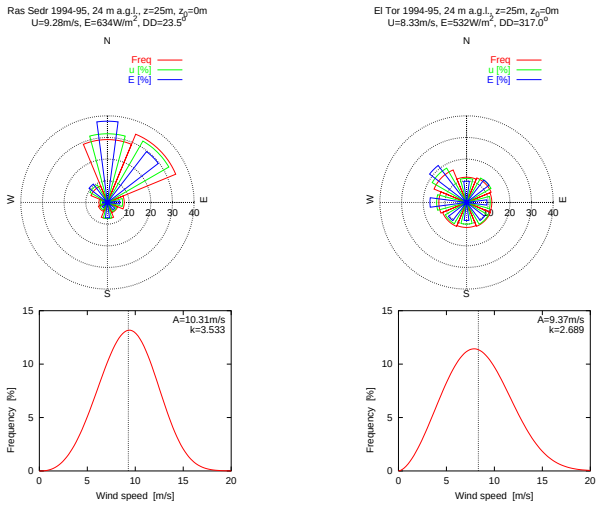

Most of the wind roses and Weibull distributions are very narrow. This is also simulated correctly (see below), though the simulated wind roses tend to be too narrow.

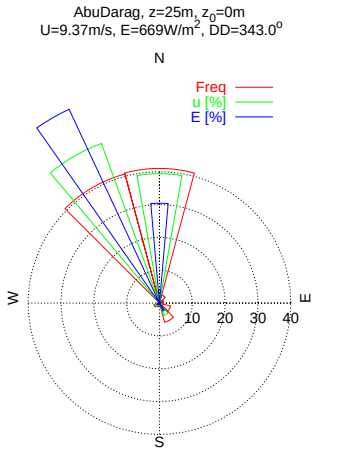
AbuDarag, z=25m, z0=0m
U=9.37m/s, E=669W/m2, DD=343.0o
N
W
E
S
Freq
u [%]
E [%]
10
20
30
40

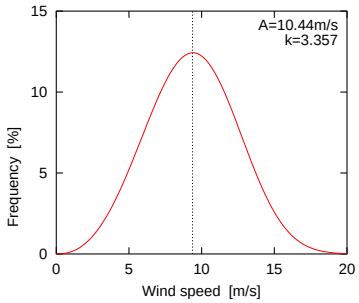
A=10.44m/s
k=3.357
Frequency [%]
Wind speed [m/s]
0
5
10
15
20

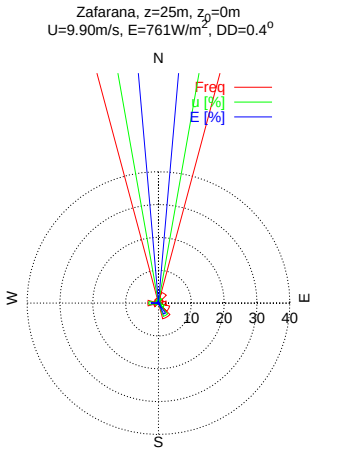
Zafarana, z=25m, z0=0m
U=9.90m/s, E=761W/m2, DD=0.4o
N
W
E
S
Freq
u [%]
E [%]
10
20
30
40

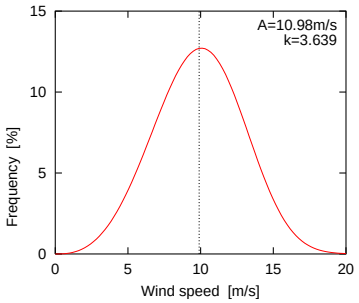
A=10.98m/s
k=3.639
Frequency [%]
Wind speed [m/s]
0
5
10
15
20

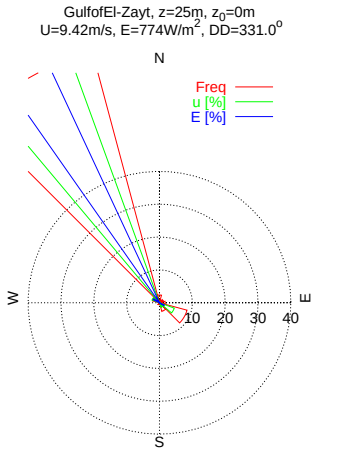
GulfofEl-Zayt, z=25m, z0=0m
U=9.42m/s, E=774W/m2, DD=331.0o
N
W
E
S
Freq
u [%]
E [%]
10
20
30
40

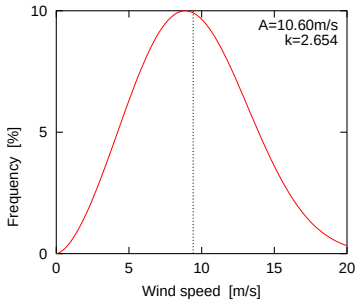
A=10.60m/s
k=2.654
Frequency [%]
Wind speed [m/s]
0
5
10
15
20

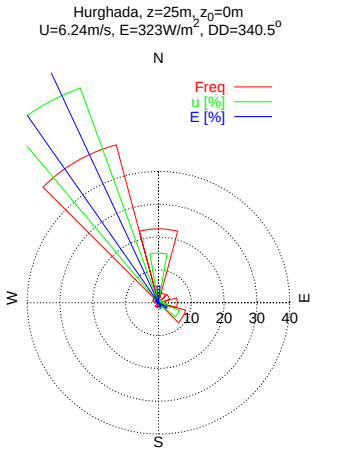
Hurghada, z=25m, z0=0m
U=6.24m/s, E=323W/m2, DD=340.5o
N
W
E
S
Freq
u [%]
E [%]
10
20
30
40

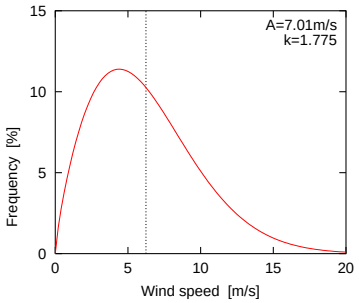
A=7.01m/s
k=1.775
Frequency [%]
Wind speed [m/s]
0
5
10
15
20

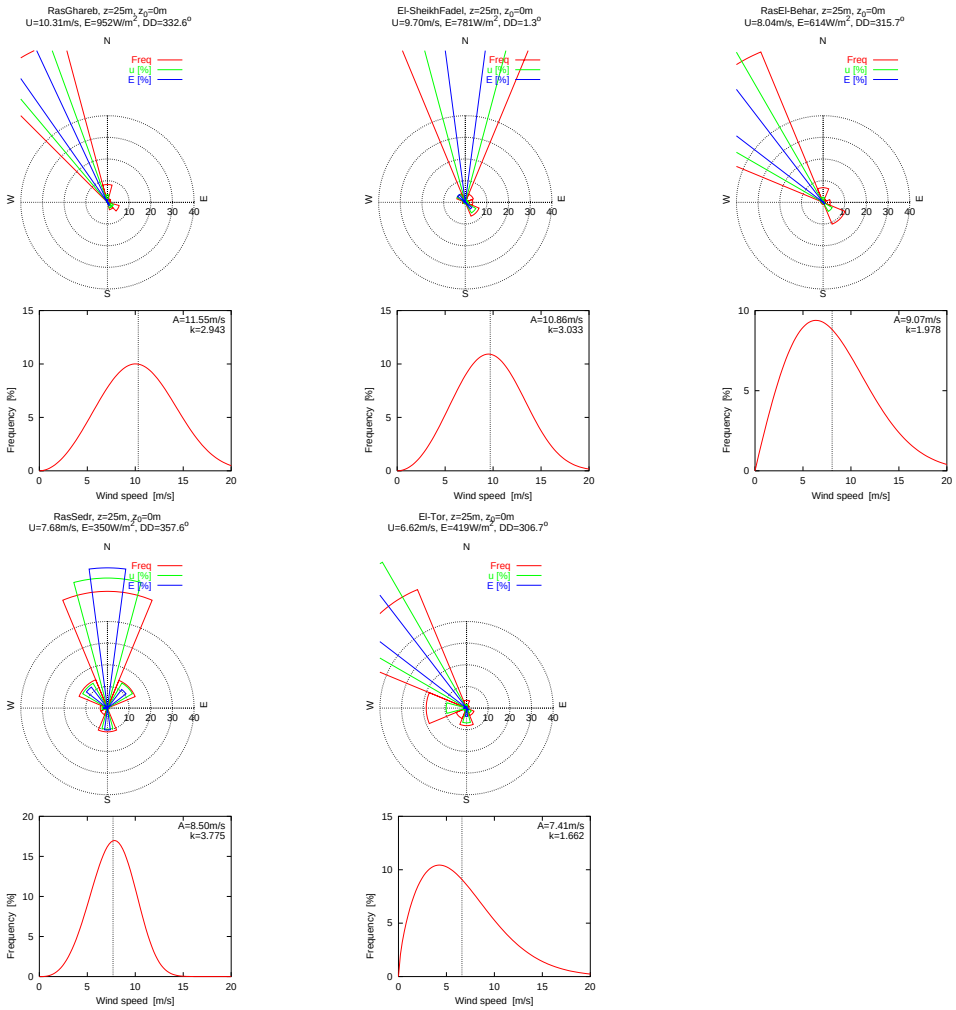

The wind speed and energy flux density at 25 m a.g.l. over roughness class 0 from observed data are listed in Table 2. The values for Abu Darag, Zafarana, El-Zayt and Hurghada differ from the numbers given in Mortensen and Said (1996), because they include newer observations. The data for the other stations is less reliable, because the observation period for these stations is only approximately one year.

The predicted mean speeds and energy densities are somewhat lower than observed ones. They are listed in Table 3. A major problem is, that the simulations predict southerly winds too often. This is also a major reason for the rapid decrease of the mean wind speed at the southern end of the Gulf. In addition, some simulations did not reach a steady state. The wind speed was still increasing in the southern part of the Gulf and in the Red Sea.

The gradients of wind speed and energy density are quite steep in the gulf area. Hence, the prediction is sensitive to the exact position of a station. This can be seen comparing the values of the neighboring grid points listed for four sites in Table 3.

For all simulations results were also saved after only 85% of the total simulation time. As the wind decreases towards the end of the simulation at some stations, somewhat higher mean winds could be obtained by assuming that this output is more realistic than the final simulation result.

Further tests must be made with different initial temperature difference of the air and the land or sea surface. A first look at calculations with no temperature difference between initial air temperature and surface temperature indicates that the mean wind would is weaker in this case. The wind rose for some stations like Hurghada or El-Tor might improve.

Another source of error could be the period of the large-scale data. Here, 34 years, from 1965 to 1998, were used. The data in Mortensen and Said (1996) was measured only during 1–8 years.

Table 2: Mean wind speed U and energy flux density E at 25 m a.g.l. over roughness class 0 ($z_0 = 0.2$mm) at 9 sites in the Gulf of Suez which are described in the Wind Atlas for the Gulf of Suez (Mortensen and Said, 1996).

Site	U [m s^{-1}]	E [W m^{-2}]	DD [°]
Abu Darag	9.88	816	358
Zafarana	10.37	966	1
Gulf of El-Zayt	11.54	1267	328
Hurghada	7.63	422	327
Ras Ghareb	10.23	918	323
El-Sheikh Fadel	8.67	546	297
Ras El-Behar	10.00	830	313
Ras Sedr	9.28	634	23
El-Tor	8.33	532	317

Table 3: Predicted mean wind speed U and energy density E at 25 m a.g.l. over roughness class 0 ($z_0 = 0.2$mm) at 9 sites in the Gulf of Suez. At the 4 main sites described in the Wind Atlas for the Gulf of Suez (Mortensen and Said, 1996) the prediction for the nearest grid point and for the next grid point to the North, East, South, and West are listed. These directions are referring to the rotated coordinates used for the simulations.

Site	U [m s^{-1}]	E [W m^{-2}]	DD [°]
Abu Darag	9.37	669	343
Abu Darag E	8.47	487	337
Abu Darag N	8.97	587	342
Abu Darag S	8.80	581	342
Abu Darag W	9.01	661	354
Zafarana	9.90	761	0
Zafarana E	9.82	778	355
Zafarana N	9.87	768	0
Zafarana S	9.91	764	0
Zafarana W	9.81	733	0
Gulf of El-Zayt	9.42	774	331
Gulf of El-Zayt E	9.59	834	329
Gulf of El-Zayt N	9.57	807	330
Gulf of El-Zayt S	9.20	785	332
Gulf of El-Zayt W	9.28	816	333
Hurghada	6.24	323	340
Hurghada E	5.12	220	334
Hurghada N	6.20	327	340
Hurghada S	6.10	307	341
Hurghada W	5.94	274	343
Ras Ghareb	10.31	952	332
El-Sheikh Fadel	9.54	751	338
Ras El-Behar	8.06	587	330
Ras Sedr	7.55	318	344
El-Tor	6.15	378	319

However, it is thought that this difference is not very big where several years of observation are available.

5 Summary

The simulations of the wind climate of the Gulf of Suez with the Karlsruhe Atmospheric Mesoscale Model KAMM capture the main features of the observed wind climate. The mean wind speed and energy flux density are somewhat underpredicted.

However, the method of generating wind atlases from the simulations is under constant development. The development is made mainly through the Danish Energy Research project "The numerical Wind Atlas – the KAMM/WASP method". New knowledge gained through this project should improve the results for the calculations on the wind climate of the Gulf of Suez.

References

G. Adrian. Zur Dynamik des Windfeldes über orographisch gegliedertem Gelände. *Ber. Deutscher Wetterdienst*, 188:142 pp, 1994.

G. Adrian and F. Fiedler. Simulation of unstationary wind and temperature fields over complex terrain and comparison with observations. *Beitr. Phys. Atmosph.*, 64:27–48, 1991.

H. P. Frank and L. Landberg. Modelling the wind climate of Ireland. *Boundary-Layer Meteorol.*, 85: 359–378, 1997.

H. P. Frank and L. Landberg. Numerical simulation of the Irish wind climate and comparison with wind atlas data. In R. Watson, editor, *Proc. EWEC'97, Dublin 1997*, pages 309–312. Irish Wind Energy Association, 1998. ISBN 0-9533922-0-1.

F. Frey-Buness, D. Heimann, and R. Sausen. A statistical-dynamical downscaling procedure for global climate simulations. *Theor. Appl. Climatol.*, 50:117–131, 1995.

E. Kalnay, M. Kanamitsu, R. Kistler, W. Collins, D. Deaven, L. Gandin, M. Iredell, S. Saha, G. White, J. Woollen, Y. Zhu, A. Leetmaa, R. Reynolds, M. Chelliah, W. Ebisuzaki, W. Higgins, J. Janowiak, K. C. Mo, C. Ropelewski, J. Wang, R. Jenne, and D. Joseph. The NCEP/NCAR 40-year reanalysis project. *Bull. Amer. Meteor. Soc.*, 77:437–471, 1996.

N. G. Mortensen and U. S. Said. *Wind Atlas for the Gulf of Suez 1991-95*. Meteorology and Wind Energy Department, Risø National Laboratory, Roskilde, Denmark, 1996. ISBN 87-550-2143-3.

Bibliographic Data Sheet **Risø-I-1970(EN)**

Title and authors

Wind Simulations for the Gulf of Suez with KAMM

Helmut P. Frank

Department or group	Date
Wind Energy Department	April 2003

Groups own reg. number(s)	Project/contract No(s)
VES 1170 104-00 MET 1105 104-00	Danida 1305/473 (104.Egypten.32)

Sponsorship

Danish Ministry of Foreign Affairs (Danida)

Pages	Tables	Illustrations	References
23	3	9	7

Abstract (max. 2000 characters)

In order to get a better overview of the spatial distribution of the wind resource in the Gulf of Suez, numerical simulations to determine the wind climate have been carried out with the Karlsruhe Atmospheric Mesoscale Model KAMM. The method and the results are described here.

The simulations of the wind climate of the Gulf of Suez with KAMM capture the main features of the observed wind climate. The mean wind speed and energy flux density are somewhat underpredicted.

Copies to: Information Service Department (2)